CLEARINGHOUSE FOR FEDERAL SCIENTIFIC AND TECHNICAL INFORMATION, CFSTI
DOCUMENT MANAGEMENT BRANCH 410.11

LIMITATIONS IN REPRODUCTION QUALITY

Accession # 603723

☑ 1. We regret that legibility of this document is in part unsatisfactory. Reproduction has been made from best available copy.

☐ 2. A portion of the original document contains fine detail which may make reading of photocopy difficult.

☐ 3. The original document contains color, but distribution copies are available in black-and-white reproduction only.

☐ 4. The initial distribution copies contain color which will be shown in black-and-white when it is necessary to reprint.

☐ 5. Limited supply on hand; when exhausted, document will be available in Microfiche only.

☐ 6. Limited supply on hand; when exhausted document will not be available.

☐ 7. Document is available in Microfiche only.

☐ 8. Document available on loan from CFSTI (TT documents only).

☐ 9.

Processor: [illegible]

NBS___ 9/64

# UNIVERSITY OF MINNESOTA
## INSTITUTE OF TECHNOLOGY

# DEPARTMENT OF AERONAUTICAL ENGINEERING





MINNEAPOLIS 14, MINNESOTA

Progress Report No 19

# THEORETICAL PARACHUTE INVESTIGATIONS



Aeronautical Systems Division Contract No. AF 33(616)-8310; Project No 6065; Task No 60252

1 September 1961 to 30 November 1961

Department of Aeronautics and Engineering Mechanics, No 5007
University of Minnesota



Dr. H. G. Heinrich, Professor, Department of Aeronautics and Engineering Mechanics
Dr. T. Riabokin, Research Associate, Department of Aeronautics and Engineering Mechanics
Prof. S. K. Ibrahim, Research Fellow, Department of Aeronautics and Engineering Mechanics
Mr. E. L. Haak, Senior Engineer, Department of Aeronautics and Engineering Mechanics
Mr. R. J. Niccum, Senior Engineer, Department of Aeronautics and Engineering Mechanics
and graduate and undergraduate students of the Department of Aeronautics and Engineering Mechanics (see Appendix)

TABLE OF CONTENTS

# THEORETICAL PARACHUTE INVESTIGATIONS

Progress Report No 19

## INTRODUCTION

1.0 This is the nineteenth quarterly report covering the time from 1 September 1961 to 30 November 1961 on the study program on basic information of Aerodynamic Deceleration.

1.1 As in preceding reporting periods, work during this reporting period has been pursued in accordance with the technical program, and is described in the following sections of this report.

## 2.0 Investigation of Wake Effects on the Behavior of Parachutes and Other Retardation Devices Behind Large Bodies at Subsonic and Supersonic Speeds

2.1 The work done on this project will be reported in three phases: a) velocity and pressure distribution in the wake of basic bodies of revolution in subsonic flow, b) drag reduction on secondary bodies in the wake of basic bodies of revolution in subsonic flow, and c) analytical analysis of turbulent wake in supersonic flow.

### 2.2 Velocity and Pressure Distribution in the Wake of Basic Bodies of Revolution in Subsonic Flow

The first phase of a general study aimed at investigating the effects of primary body wake upon the operation and performance of aerodynamic decelerators in subsonic flow consisted of deriving, through theoretical analysis, the velocity and pressure distribution in the wake of basic bodies of revolution, as reported in Ref 1. A subsequent study was reported in Ref 2.

In order to verify this theory, an extensive experimental study was made, and the results of this study, together with a comparison of experimental and theoretical results were presented in Progress Report No 17. An analysis of this comparison was made in Progress Report No 18.

Work during the present reporting period has been devoted toward the drafting of a technical report summarizing the results of experimental and theoretical work performed thus far on primary body wake in subsonic flow.

The next period will be devoted to work on this technical report.

## 2.3 Drag Reduction on Secondary Bodies in the Wake of Basic Bodies of Revolution in Subsonic Flow

The goal of this study is the prediction of the drag reduction on secondary bodies in the wake of primary bodies. The first effort consisted of an experimental study comparing the drag of several secondary bodies in free stream with their drag at various positions in the wake of a primary body in subsonic flow. The final results of this study, together with a complete discussion, were presented in Ref 3.

Efforts now turn to an analytical investigation of the drag reduction of secondary bodies in the wake of a primary body based on the experimental data above. Progress Report No 18 presented a general outline for this analytical study, based on observations of the experimental results. During this reporting period, this analysis has been pursued, following the outline of Progress Report No 18. These efforts will be continued during the next period.

## 2.4 Analytical Analysis of Turbulent Wake in Supersonic Flow

### 2.4.1 Introduction

For transonic and supersonic flow, the first step in the investigation of the effects of primary body wake upon the operation and performance of aerodynamic decelerators in supersonic flow was an extensive experimental study of primary body, secondary body, and combination drag, and pressure and velocity distribution in the wake. Final technical reports are being written on these results which will furnish a basis for theoretical studies.

The first step in the theoretical treatment is an analysis of the variation of pressure, velocity, density, and temperature in the wake of an axially symmetric body. This analysis begins with the development of the governing equations for compressible flow, the equations of continuity, momentum, energy, and state of fluid.

The flow is assumed to be axially symmetric, with no rotation about the longitudinal axis. Furthermore, the fluid will be assumed to be a perfect gas with constant specific heats. A cylindrical coordinate system as shown in Fig 1-1 is used. Velocity components are shown in Fig 1-2.

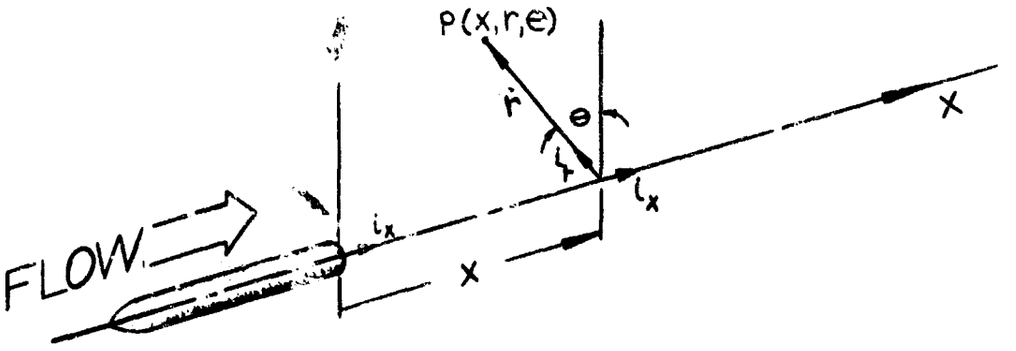


FIG 1-1. CYLINDRICAL COORDINATE SYSTEM FOR WAKE ANALYSIS

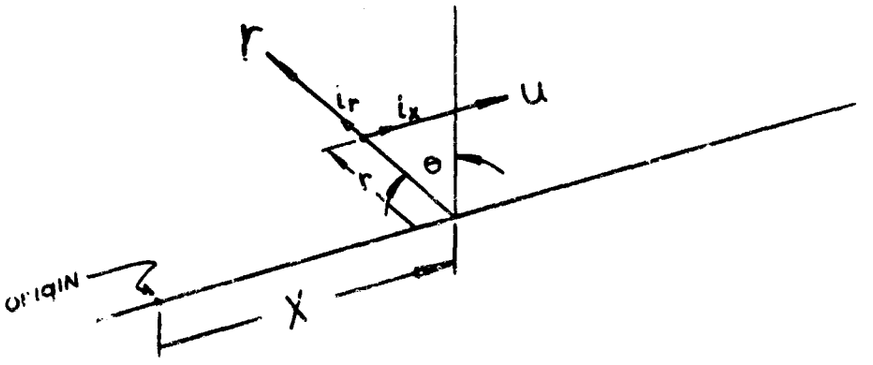


FIG 1-2. VELOCITY COMPONENTS IN CYLINDRICAL COORDINATES

2.4.2 List of Symbols

$c_v$ = specific heat of fluid at constant volume
D/Dt = total or material derivative
d = characteristic length of body
e = internal energy of fluid per unit mass
$\vec{F}$ = body forces on a fluid particle (gravity, etc)
$\hat{i}_x$ = unit vector in axial direction

$\hat{i}_r$ = unit vector in radial direction
$\hat{i}_\theta$ = unit vector in transverse direction
K = thermal conductivity of fluid
p = static pressure of fluid at a point
r = distance in the radial direction
r* = dimensionless radial distance r/d
T = temperature of the fluid at a point
t = time
u = velocity in the axial direction
$\vec{V}$ = fluid velocity at a point
v = velocity in the radial direction
w = velocity in the transverse direction ( = 0)
x = distance in the axial direction
x* = dimensionless axial distance
$\rho$ = fluid density at a point
$\vec{\vec{\tau}}_m$ = mechanical stress tensor
$\tau_{rx}$ = shearing stress in axial direction
$\tau_{rx_T}$ = turbulent shearing stress in axial direction
$\tau_{xr}$ = shearing stress in radial direction
$\tau_{xr_T}$ = turbulent stress in radial direction
$\nabla$ = del operator
$\overline{(\ )}$ = time average of fluid particle property ( ) at any point in the flow field
$(\ )'$ = fluctuating component of ( ) at any point in the flow field
$\overline{\overline{(\ )}}$ = defect of ( ) from its free stream value
$(\ )^*$ = dimensionless value of $\overline{(\ )}$ $\left[= \overline{(\ )}/(\ )_\infty\right]$

2.4.3 Basic Equations

The continuity equation (conservation of mass) for axially symmetric flow without rotation of a compressible viscous fluid can be written in vector form as

$$\frac{\partial \rho}{\partial t} + \nabla\cdot(\rho\vec{V}) = 0 \qquad (1.1a)$$

or, expanding in cylindrical coordinates

$$\frac{\partial \rho}{\partial t} + \frac{1}{r}\frac{\partial}{\partial r}(\rho r v) + \frac{1}{r}\frac{\partial}{\partial x}(\rho r u) = 0 . \tag{1.1b}$$

The momentum equation in vector form is

$$\rho \frac{D\vec{V}}{Dt} = \nabla \cdot \vec{\vec{\tau}}_m + \rho \vec{F} , \tag{1.2a}$$

where

$$\frac{D(\ )}{Dt} = \frac{\partial(\ )}{\partial t} + \vec{V} \cdot \nabla(\ ) . \tag{1.3}$$

If we are considering flow of a gas (such as air) we may neglect the body force $\vec{F}$. Also, for axially symmetric flow without rotation, we may write the stress tensor (Ref 4) as

$$\vec{\vec{\tau}}_m = -p\vec{\vec{I}} + \vec{\vec{\tau}} , \tag{1.4}$$

where

$$\vec{\vec{I}} = \hat{i}_r \hat{i}_r + \hat{i}_x \hat{i}_x ,$$
$$\vec{\vec{\tau}} = \hat{i}_r \hat{i}_x \tau_{rx} + \hat{i}_x \hat{i}_r \tau_{xr} .$$

Then, noting that derivatives of quantities with respect to $\theta$ are zero, it can be shown that in cylindrical coordinates

$$\nabla \cdot \vec{\vec{\tau}}_m = \hat{i}_r \left( \frac{\partial \tau_{xr}}{\partial x} - \frac{\partial p}{\partial r} \right) + \hat{i}_x \left[ \frac{1}{r}\frac{\partial}{\partial r}(r \tau_{rx}) - \frac{\partial p}{\partial x} \right] . \tag{1.5}$$

Substituting this result, and expanding the left side of Eqn (1.2a) yields the momentum equation

$$\hat{i}_r \left[ \rho \left( \frac{\partial v}{\partial t} + u\frac{\partial v}{\partial x} + v\frac{\partial v}{\partial r} \right) - \frac{\partial \tau_{xr}}{\partial x} + \frac{\partial p}{\partial r} \right] + \tag{1.2b}$$

$$+ \hat{i}_x \left[ \rho \left( \frac{\partial u}{\partial t} + u\frac{\partial u}{\partial x} + v\frac{\partial u}{\partial r} \right) - \frac{1}{r}\frac{\partial}{\partial r}(r \tau_{rx}) + \frac{\partial p}{\partial x} \right] = 0 .$$

This vector equation may be written as two scalar equations for the x and r directions.

The energy equation in vector form, neglecting body forces is

$$\rho \frac{D}{Dt}\left(e + \frac{V^2}{2}\right) = \nabla\cdot\left(\overline{\overline{\tau}}_m \cdot \vec{V}\right) + \nabla\cdot\left(k\nabla T\right). \qquad (1.6a)$$

In cylindrical coordinates, for axially symmetric flow of a perfect gas with no rotation about the longitudinal axis, this expands to

$$\rho\left(\frac{\partial}{\partial t} + u\frac{\partial}{\partial x} + v\frac{\partial}{\partial r}\right)\left(c_v T + \frac{u^2+v^2}{2}\right) = \frac{1}{r}\frac{\partial}{\partial r}\left[r\left(u\tau_{rx} - pv\right)\right] + \qquad (1.6b)$$

$$+ \frac{1}{r}\frac{\partial}{\partial x}\left[r\left(v\tau_{xr} - pu\right)\right] + \frac{k}{r}\left[\frac{\partial}{\partial r}\left(r\frac{\partial T}{\partial r}\right) + \frac{\partial}{\partial x}\left(r\frac{\partial T}{\partial x}\right)\right].$$

The equation of state for a perfect gas is

$$p = \rho R T. \qquad (1.7)$$

Equations (1.1b), (1.2b), (1.6b), and (1.7) form a set of partial differential equations which specify the flow field in an axially symmetric wake.

2.4.4 Simplification of Equations

Since most instruments presently used in experimental aerodynamics measure average quantities of density, velocity, etc., it is advantageous to write the above equations in terms of average flow quantities. Therefore, we define the instantaneous flow quantities as the sum of a local average quantity and a small fluctuating quantity as follows:

$$\begin{aligned} u &= \bar{u} + u', \\ v &= \bar{v} + v', \\ p &= \bar{p} + p', \\ \rho &= \bar{\rho} + \rho', \\ T &= \bar{T} + T'. \end{aligned} \qquad (1.8)$$

If these relations are substituted into the set of partial differential equations, and a time average is taken, a number of terms of the form $\overline{\rho' u' \partial v'/\partial x}$ are obtained. These terms are not generally equal to zero. Therefore, these terms are lumped into new shear stresses, which together with the mechanical shear stresses make up the turbulent shear stresses.

At present, it is impossible to solve the set of equations as obtained by substituting Eqn (1.8). In order to obtain a solution, we make changes of variables as follows:

$$\begin{aligned} \overline{u} &= U_\infty + \overline{u}, \\ \overline{v} &= \overline{v}, \\ \overline{p} &= p_\infty + \overline{p}, \\ \overline{\rho} &= \rho_\infty + \overline{\rho}, \\ \overline{T} &= T_\infty + \overline{T}. \end{aligned} \tag{1.9}$$

We make the assumptions: $\overline{u} \ll U_\infty$, $\overline{v} \ll U_\infty$, $\overline{p} \ll p_\infty$, $\overline{\rho} \ll \rho_\infty$, and $\overline{T} \ll T_\infty$. We also assume that the average flow quantities are independent of time. Introduction of these relations into the modified set of equations and neglecting second order terms gives a set of linear equations.

It proves advantageous to reduce the set of linear equations to a dimensionless form. We do this by introducing the dependent and independent dimensionless variables:

$$\begin{aligned} \rho^* &= \rho/\rho_\infty \\ u^* &= \overline{u}/U_\infty, \\ v^* &= \overline{v}/U_\infty, \\ p^* &= \overline{p}/p_\infty, \\ T^* &= \overline{T}/T_\infty, \\ x^* &= x/d, \\ r^* &= r/d. \end{aligned} \tag{1.10}$$

Introducing now Eqns (1.8), (1.9), and (1.10), along with turbulent shear stresses, and neglecting second order terms, we obtain a set of linear, dimensionless partial differential equations specifying the flow field as follows:

Continuity equations:

$$\frac{\partial u^*}{\partial x^*} + \frac{1}{r^*}\frac{\partial}{\partial r^*}\left(r^* v^*\right) + \frac{\partial \rho^*}{\partial x^*} = 0 \,, \tag{1.1c}$$

x - Momentum equation:

$$\frac{\partial u^*}{\partial x^*} = -\frac{p_\infty}{\rho_\infty U_\infty^2}\frac{\partial p^*}{\partial r^*} + \frac{1}{r^*}\frac{\partial}{\partial r^*}\left(r^* \frac{\tau_{rx_T}}{\rho_\infty U_\infty^2}\right) \,, \tag{1.2c}$$

r - Momentum equation:

$$\frac{\partial v^*}{\partial x^*} = -\frac{p_\infty}{\rho_\infty U_\infty^2}\frac{\partial p^*}{\partial r^*} + \frac{\partial}{\partial x^*}\left(\frac{\tau_{xr_T}}{\rho_\infty U_\infty^2}\right) \,, \tag{1.2d}$$

Energy equation:

$$\frac{\partial T^*}{\partial x^*} + \gamma(\gamma-1)M_\infty^2 \frac{\partial u^*}{\partial x^*} = \frac{\gamma(\gamma-1)}{r^*} M_\infty^2 \frac{\partial}{\partial r^*}\left(r^* \frac{\tau_{rx_T}}{\rho_\infty U_\infty}\right) -$$

$$-\frac{\gamma-1}{r^*}\frac{\partial}{\partial r^*}(r^* v^*) + \gamma(\gamma-1)M_\infty^2 \frac{\partial}{\partial x^*}\left(v^* \frac{\tau_{xr_T}}{\rho_\infty U_\infty^2}\right) - \tag{1.6c}$$

$$-(\gamma-1)\frac{\partial u^*}{\partial x^*} - (\gamma-1)\frac{\partial p^*}{\partial x^*} + \frac{K}{r^* d \rho_\infty U_\infty C_v}\left[\frac{\partial}{\partial r^*}\left(r^* \frac{\partial T^*}{\partial r^*}\right) + r^* \frac{\partial^2 T^*}{\partial x^{*2}}\right] .$$

2.4.5 Proposed Work

Work during the next period will be devoted to an attempt to solve the velocity, pressure, density, and temperature distribution in the turbulent wake of a body in supersonic axially symmetric flow.

## REFERENCES


1. Heinrich, H. G. and Riabokin, T.: Analytical and Experimental Considerations of the Velocity Distribution in the Wake of a Body of Revolution, WADC TR 60-257, December, 1959.

2. Rubbert, Paul E.: Investigation of the Velocity Distribution in the Wake of an Axially Symmetric Body, Master's Thesis, July, 1960, University of Minnesota.

3. Heinrich, H. G. and Haak, E. L.: The Drag of Cones, Plates, and Hemispheres in the Wake of a Forebody in Subsonic Flow, ASD TR 61-587, October, 1961.

4. Prandtl, L. and Tietjens, O. G.: Fundamentals of Hydro- and Aeromechanics, McGraw-Hill Book Company, Inc. New York, 1934.

Project No 4

## 3.0 Investigation of Basic Stability Parameters of Conventional Parachutes

### 3.1 Theoretical Investigation of the Dynamic Stability of Parachutes.

Progress Report No 18 presented the derivation of the differential equations of the laterally disturbed motion of a system of parachute and store under certain simplifying assumptions. That report also presented the derivation of the frequency equation for this system of differential equations, and determined all quantities of this equation in terms of known aerodynamic coefficients and physical constants. Upon numerical evaluation of the various quantities for each system under consideration, the frequency equation can be solved, and consequently the lateral motion of that system determined.

During this reporting period, work has been devoted to a critical review of this complicated dynamic problem, with a careful check for possible errors in the analysis. It is anticipated that the next progress report will present any required modifications, together with an application to specific systems.

### 3.2 Wind Tunnel Investigation of Parachute Models

The final draft of the technical report entitled "Stability and Drag of Parachutes with Varying Effective Porosity," has been submitted to the Procuring Agency for approval.

### 3.3 Effective Porosity Studies

Porosity studies previously completed have yielded a wide range of information on the effective porosity of parachute cloths for sub-critical pressure ratios and altitudes above 50,000 ft. A facility has also been constructed

(see Progress Reports No 16, Sec 3.4.3, and No 18, Sec 3.4.2) which is capable of extending the test range for cloths over a density range of $0.10 \leq \sigma \leq 1$ and a pressure ratio range of $0.1 \leq \Delta p/\Delta p_{cr} \leq 1.2$, and tests in these ranges were initiated for four common parachute cloths.

In the course of testing, it was found that the shape and size of the cloth specimen and the particular piece of cloth being tested have an effect on the porosity at a given test condition. Therefore, standard test samples were made up and permanently mounted, thus insuring that a standard specimen is used for the entire test range for each cloth.

Tests have been continued for the density and pressure ranges above using these standard cloth specimens, and it is anticipated that results will be available for presentation in the next progress report. Also, the effects of size and shape will be discussed.

## 4.0 Theoretical Study of Supersonic Parachute Phenomena

### 4.1 Introduction

This study has analyzed the behavior of conventional parachutes in supersonic air flow and using the water analogy. Based on this analysis, a supersonic deceleration device was conceived which utilizes a pressure reducing "spike." The continuing development and testing of this spiked parachute has been pursued during this reporting period in the following phases:

a) Supersonic wind tunnel studies of flexible spiked parachutes
b) Pressure distribution studies on spiked parachute in supersonic flow.

These phases will be reported in respective order in the following sections of this report.

### 4.2 Supersonic Wind Tunnel Tests of Flexible Spiked Parachutes

#### 4.2.1 Past Work

Rigid models of the spiked parachute have been found stable in wind tunnel tests at Mach numbers of 1.14, 2.0, and 3.0, both with and without suspension lines. Progress Reports Nos 17 and 18 reported results of initial tests on configurations of this parachute with flexible textile canopies.

In these initial tests, both the model and the tunnel suspension system suffered mechanical damage. This prompted design of a new tunnel suspension system and a deployment device which were described extensively in Progress Report No 18.

#### 4.2.2 Continuation

Tests have been continued during the present reporting period on the spiked parachute with flexible canopy. The deployment device has functioned very well during these tests, and

damage to the canopy during deployment has been eliminated. Furthermore, canopy cloth failure near the gore seams has been eliminated through the use of heavier MIL-C-8021A, Type II nylon cloth (300 lb/in) with the canopy design shown in Fig 7-7 of Progress Report 18. These canopies have proven very durable, often surviving several tests at Mach 3.0.

Another source of mechanical damage during testing was the failure of the wire rings which had been inserted into the leading edge of the canopy as an aid to inflation. These wires had either broken, initiating tears in the cloth, or had suffered permanent deformation during the deployment. Since such a wire ring is not generally desirable, on several tests made during this period the wire rings were omitted. In these tests, the model seemed to inflate very well, but was slightly less stable than with wire ring. Figure 7-1 presents a Schlieren photograph of a flexible model in Mach 3 flow without the wire ring.

In recent tests a third mode of failure occurred; namely, the suspension lines separated from the canopy and the cone. In each case, the separation seemed to occur near the end of the test run, indicating a gradual weakening rather than an immediate failure. To avoid this a new suspension line system has been introduced (Fig 7-2) which is essentially the same as shown in Fig 7-8 of Progress Report No 18, except that instead of each line being an individual piece, the entire set of lines is made up of one continuous line.

In addition to the canopy design mentioned above, a second canopy design, consisting only of a truncated cone was tested. Progress Report No 17 shows this canopy, designated Canopy C, in Fig 7-3 and presents results of water analogy studies, where the canopy showed promising characteristics. However, in the wind tunnel tests at Mach 3, the model was violent unstable.

### 4.2.3 Proposed Work

Supersonic wind tunnel tests will be continued to further improve the spiked parachute. Specifically, studies

will continue on models without the wire ring in the leading edge.

## 4.3 Pressure Distribution Studies on Spiked Parachute In Supersonic Flow

### 4.3.1 Introduction

During this reporting period, initial pressure distribution studies were made on rigid models of the spiked parachutes in the supersonic wind tunnel at Mach 3.0. It is hoped that such pressure distribution studies will yield information which will be helpful in the modification of flexible canopies so that better performance can be obtained.

### 4.3.2 Models and Test Procedure

The rigid models used were the same as those previously used in stability studies (see Progress Report No 14, Fig 7-1). One model has 14 static pressure taps diametrically opposed for measuring external pressure on the canopy, plus six taps on the base of the cone. A second model has 14 taps diametrically opposed to measure internal pressure on the canopy, plus four taps on the sting between the cone and canopy. The taps on the base of the cone and on the sting are to determine the amount of pressure recovery in the wake area of the cone. The test arrangement is shown in Fig 7-3.

Three tests were made on each model without suspension lines, and then suspension lines were added for three more tests to determine their effect. Pressures were measured on a multiple manometer and photographed during each test. High speed Schlieren movies were made of each test run.

### 4.3.3 Results

The pressure measurements from the three tests of the internal and external tap models were averaged in each case,

for tests both with and without suspension lines. These measurements were reduced to coefficient form with the pressure coefficient, $C_p$, defined as

$$C_p = \frac{P_L - P_S}{q}$$

where $P_L$ = local pressure on surface of model
$P_S$ = free stream static pressure
$q$ = free stream dynamic pressure.

The pressure coefficients for models both with and without suspension lines are shown in Fig 7-4. We see that the suspension lines uniformly decrease the base pressure on the cone and the pressure on the sting slightly. They have very little effect on the external pressure distribution. The lines seem to decrease the internal pressure on the forward part of the canopy, while increasing it on the rearward portion. Figures 7-5 and 7-6 show the pressure distribution on the supersonic parachute with and without suspension lines, respectively. It can be seen that the pressure distribution is of the form required for canopy inflation.

Schlieren photographs of the external tap model without suspension lines and the internal tap model with suspension lines are presented in Figs 7-7 and 7-8 respectively. The lines seen extending from the rear of the canopy in Fig 7-8 are pressure tubes.

4.3.4 Proposed Work

During the next reporting period, wind tunnel tests will be made at M = 2 as well as with a forebody in order to investigate its influence upon the pressure distribution of the spiked parachute.

A model is being constructed (see Fig 7-9) with pressure taps along the entire length of the central sting of the

parachute to determine the pressure distribution throughout the wake area of the cone. This model will also be tested during the next period.

The results of tests made thus far will be analyzed for possible application to flexible models.

FIG 7-1. FLEXIBLE SUPERSONIC PARACHUTE AT MACH 3.0 WITHOUT WIRE RING IN LEADING EDGE. 300 LB/IN NYLON CANOPY, $H/D_1 = 0.68$, $D_o/D_1 = 0.90$, $1/D_1 = 0.35$.

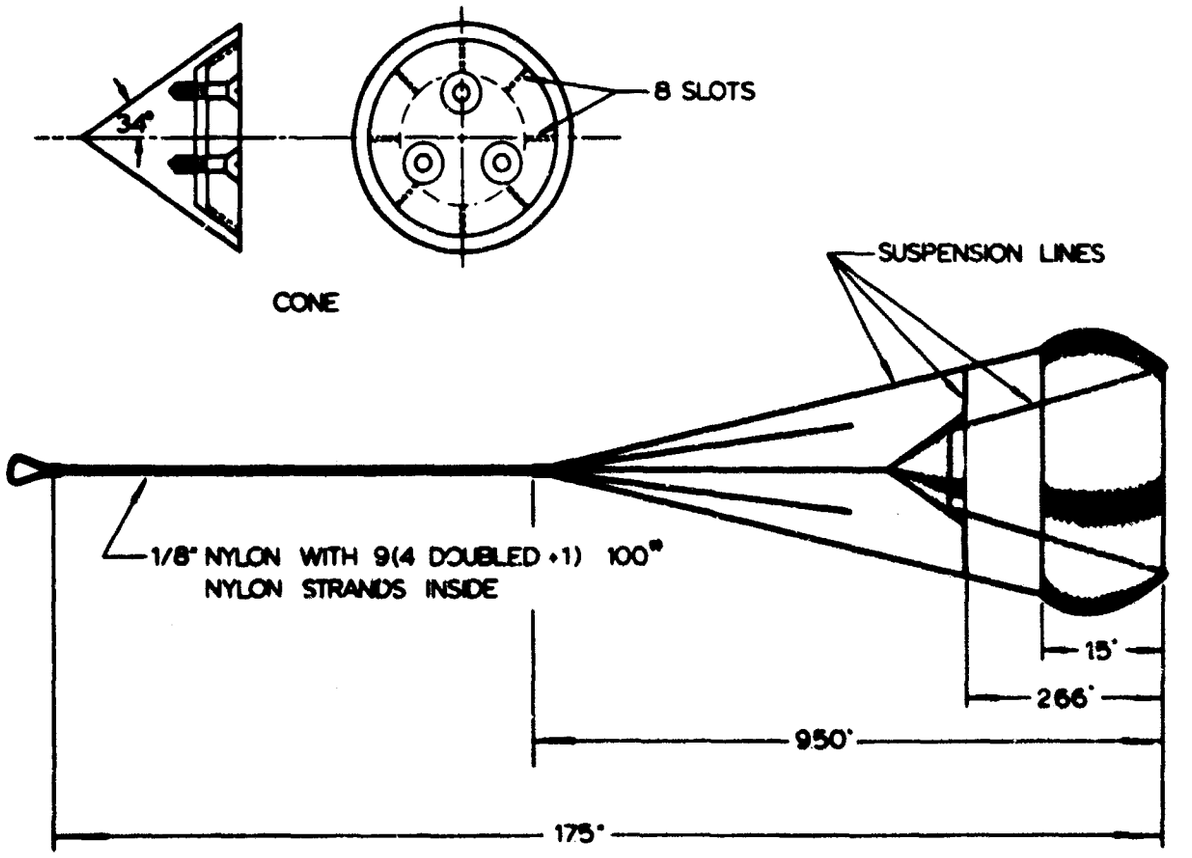


FIG 7-2. SUSPENSION LINE SYSTEM OF SUPERSONIC PARACHUTE MODEL - FOURTH DESIGN

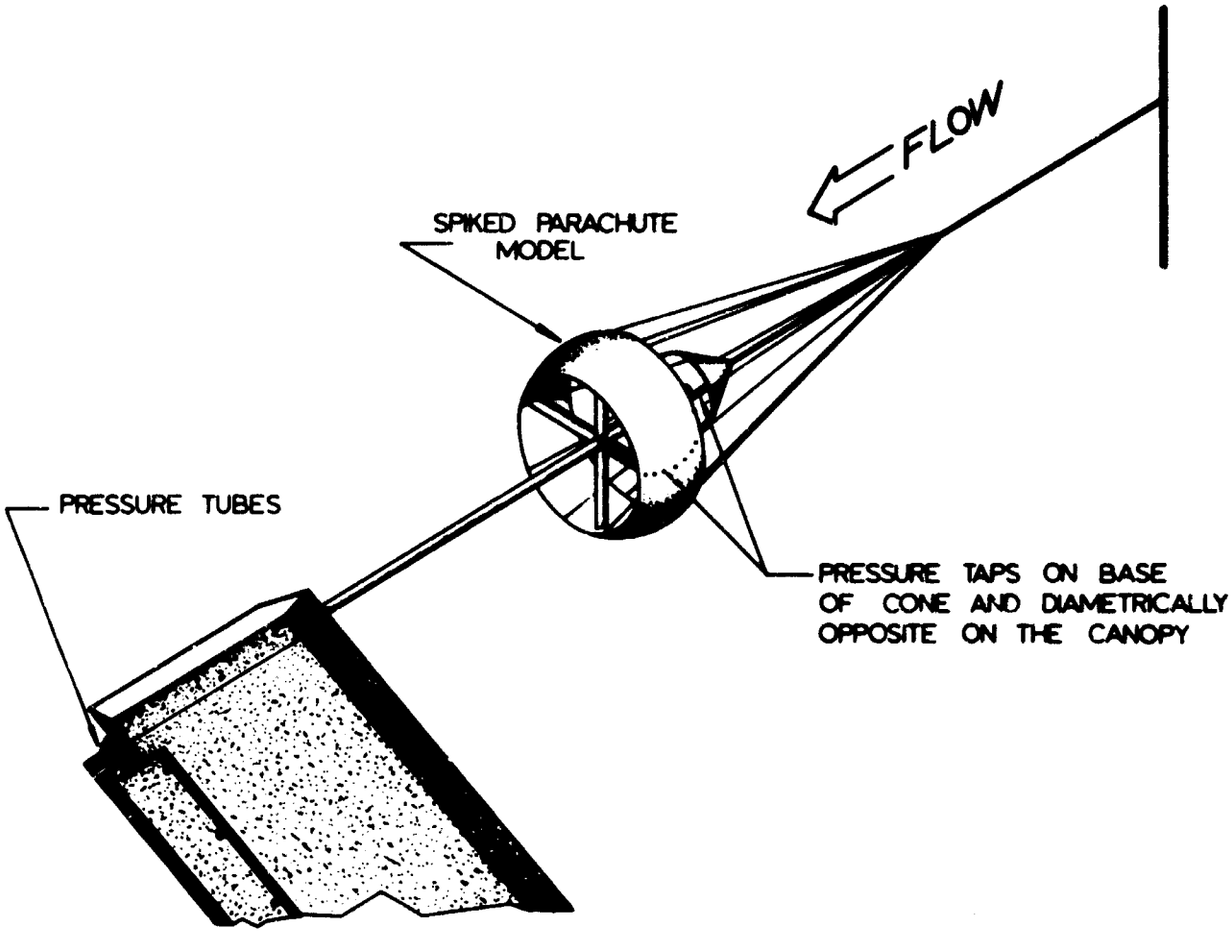


FIG 7-3. TEST ARRANGEMENT FOR PRESSURE DISTRIBUTION STUDIES ON SPIKED PARACHUTE

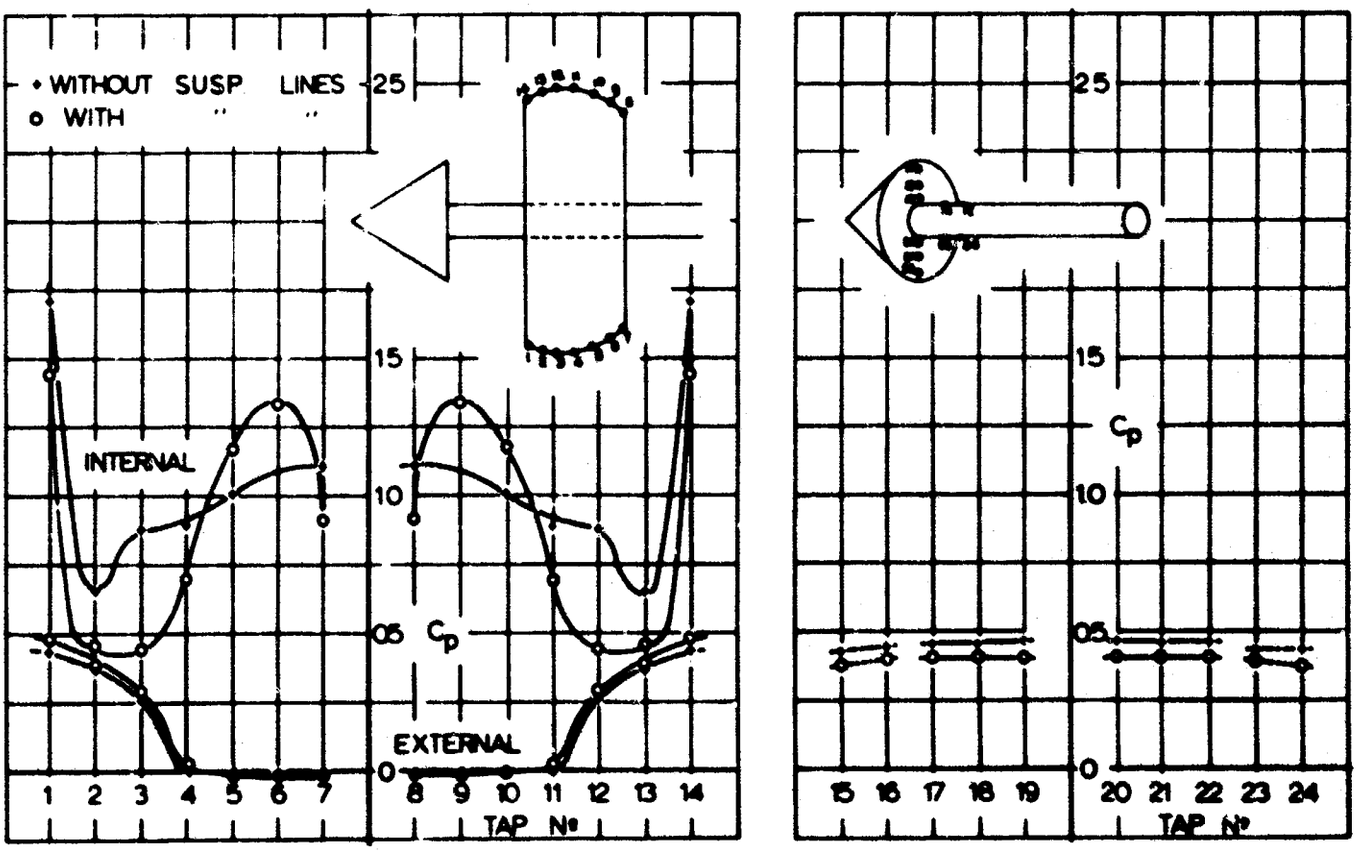


FIG 7-4. PRESSURE COEFFICIENT DISTRIBUTION ON SPIKED PARACHUTE IN FREE STREAM AT MACH 3

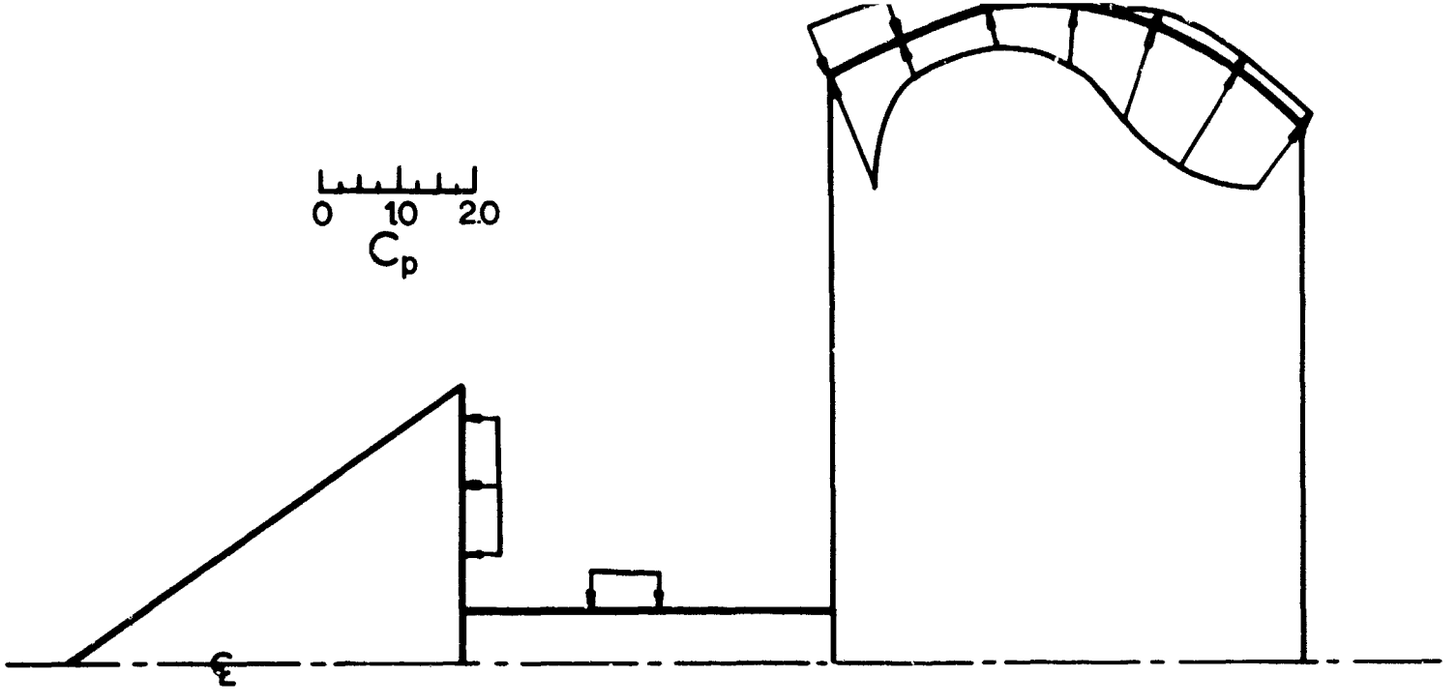


FIG 7-5. SCHEMATIC PRESSURE COEFFICIENT DISTRIBUTION ON SPIKED PARACHUTE (WITH SUSPENSION LINES)

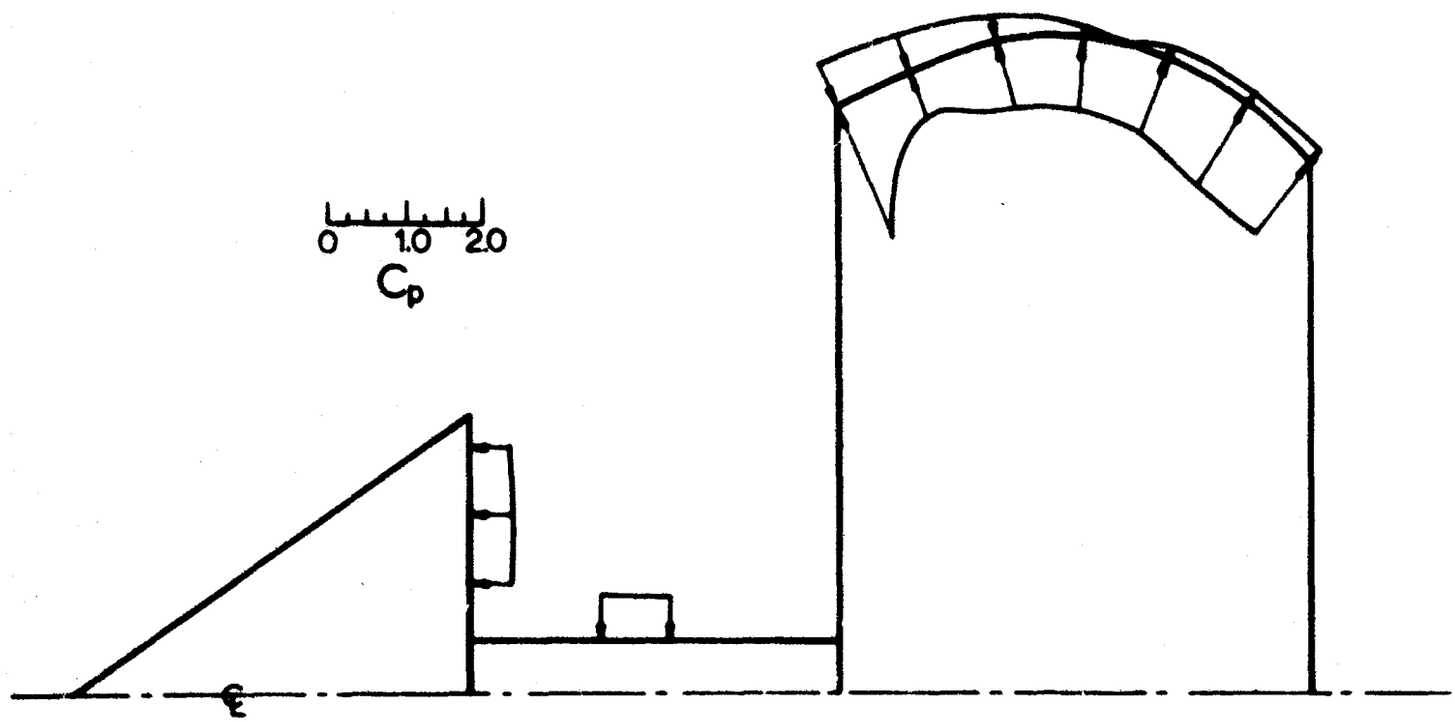


FIG 7-6. SCHEMATIC PRESSURE COEFFICIENT DISTRIBUTION ON SPIKED PARACHUTE (WITHOUT SUSPENSION LINES)

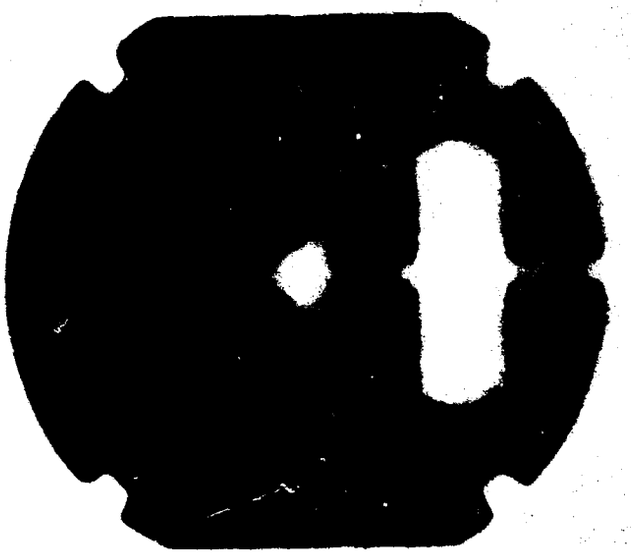

FIG 7-7. EXTERNAL TAP PRESSURE DISTRIBUTION MODEL AT MACH 3.0 WITHOUT SUSPENSION LINES.

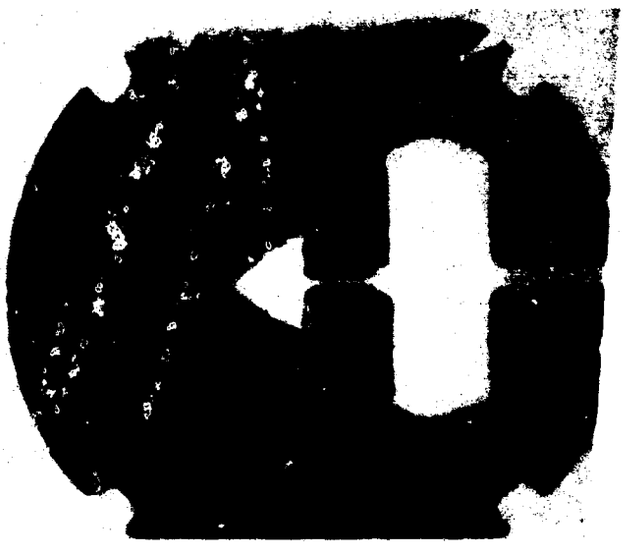

FIG 7-8. INTERNAL TAP PRESSURE DISTRIBUTION AT MACH 3.0 WITH SUSPENSION LINES.

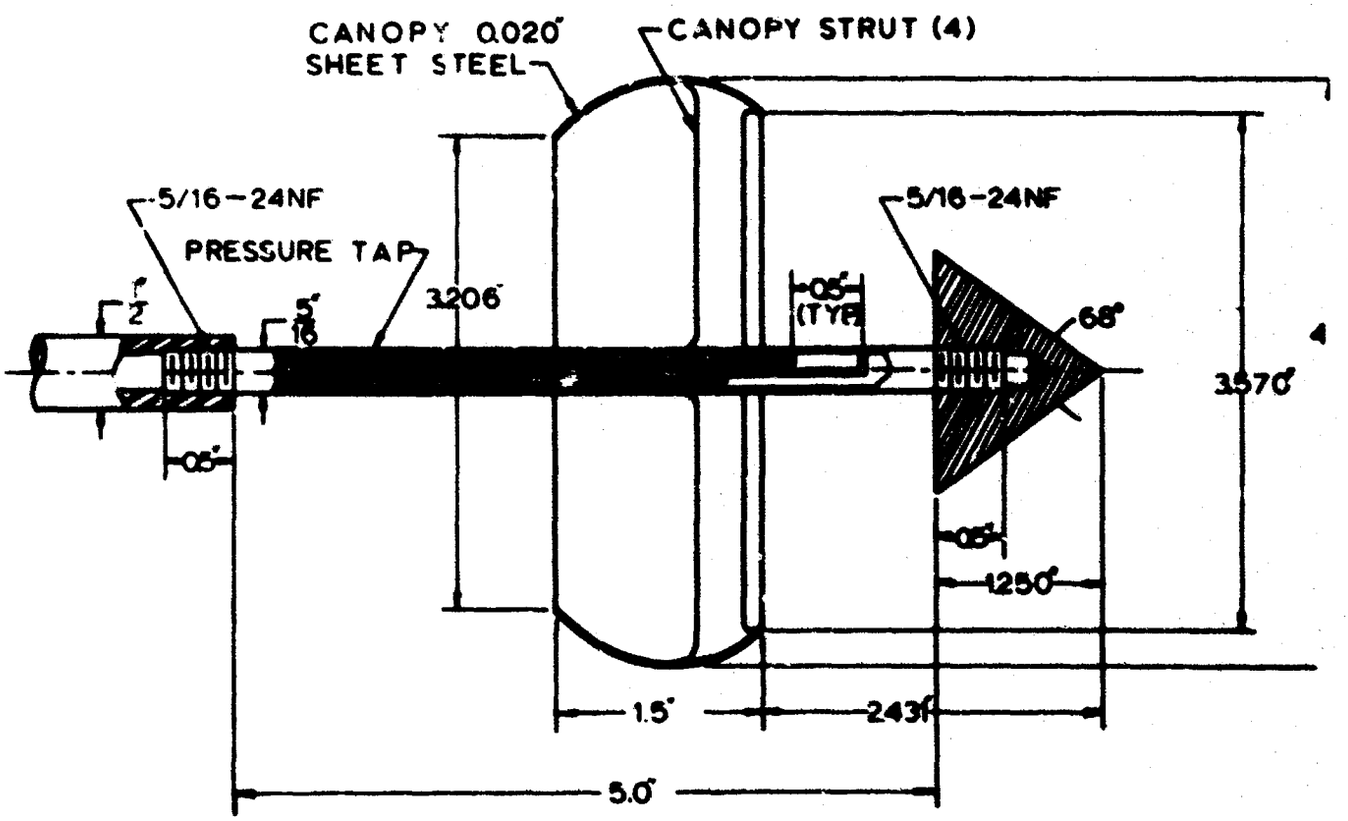


FIG 7-9 RIGID SPIKED PARACHUTE MODEL FOR MEASUR PRESSURE DISTRIBUTION ON STING.

## 5.0 Theoretical Analysis of the Dynamics of the Opening Parachute

### 5.1 Analytical Investigation of Parachute Inflation Time and Opening Force

The objective of this study is to develop an analytical method which can be used to determine the filling time and opening shock of a parachute under known operating conditions of altitude and velocity. To a certain extent, this objective has been completed, and is presented in Progress Reports No 16 and 17.

The next steps will be the application of this analytical method to parachutes with inherent geometric porosity and also to parachutes operating with a reefed canopy. An investigation will also be made of the influence of the canopy vent, which has previously been neglected, on the results of the analytical method. It is anticipated that work on these modifications will begin during the next reporting period.

### 5.2 Size-Force History of an Inflating Parachute

The above analytical method was based on specific assumptions of the drag area-time relationship. The objective of this study is to verify these assumptions experimentally.

Progress Report No 18 presented initial results of projected area versus time for a 3 ft nominal diameter circular flat parachute in the finite mass case. These results showed that except for the very early portion of the opening sequence, the projected area does vary parabolically with time, thus verifying one of the previously used assumptions.

During this reporting period, wind tunnel studies were continued on the same model to determine the variation of drag coefficient with time during the opening process.

This was done by simultaneously recording the projected area with a high speed camera and force with an electronic strain gage balance as a function of time.

When reducing the data from tests, it was found that the time coordinate on the force-time and distance-time histories was not the same as on the area-time history. To provide this required common time origin, a strobe light was placed downstream from the test section in the field of view of the high speed movie camera. Thereafter, when the parachute was disreefed, the strobe light was simultaneously activated, giving a common time origin for the three recordings.

Several wind tunnel tests were continued using this modification, but the data reduction is not complete. These results will be presented in the next progress report. Also, similar force-size studies will be made for a 10% extended skirt parachute.

## 6.0 Statistical Analysis of Extraction Time, Deployment Time, Opening Time, and Drag Coefficient for Aerial Delivery Parachutes and Systems

The second draft of the technical report for this project is currently being written.

## 7.0 Study of Basic Principles of New Parachutes and Retardation Devices

### 7.1 Introduction

The objective of this study is the investigation of the conventional ribbon parachute in combination with a wake producing "spike." This spike, which was conceived in conjunction with a supersonic parachute (see Project No 7) consists of a wedge in two-dimensional flow and a cone in three dimensional flow.

The immediate aim is to determine stability, pressure distribution, and inflation characteristics of various configurations of the spike-ribbon parachute. Initial tests were made in the water tow using the principles of the water analogy, and Progress Report No 18 presented extensive results of these tests for several configurations.

### 7.2 Continuation

During this reporting period, designs were made for both solid and flexible spiked ribbon parachute models (see Figs 10-1 through 10-6) based on the results of the water analogy studies. The canopies have geometric porosities of 20, 25, and 30 per cent. Profile shapes for the rigid models were determined previously and presented in Progress Report No 11. These rigid and flexible models are presently being constructed.

### 7.3 Proposed Work

During the next period, the models above will be tested in the wind tunnel in an initial attempt to determine stability and inflation characteristics of various spike-ribbon parachute configurations.

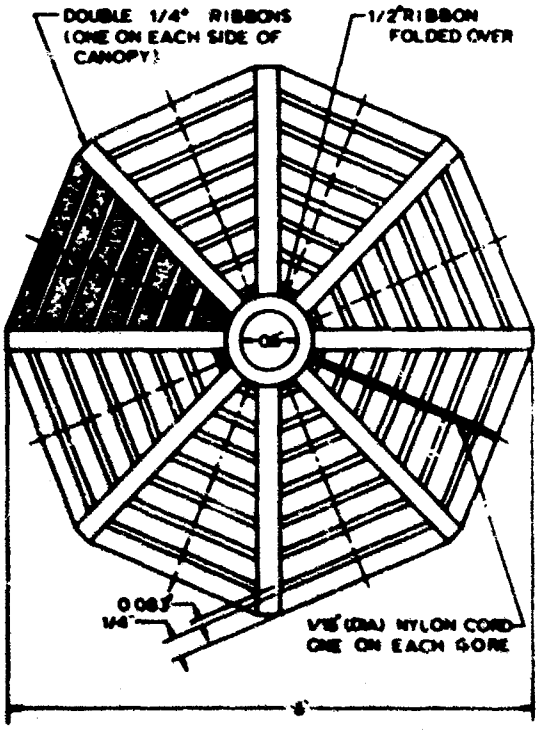


FIG 10-1 FLEXIBLE CANOPY DESIGN FOR SPIKED RIBBON PARACHUTE CONFIGURATION (20% GEOMETRIC POROSITY)

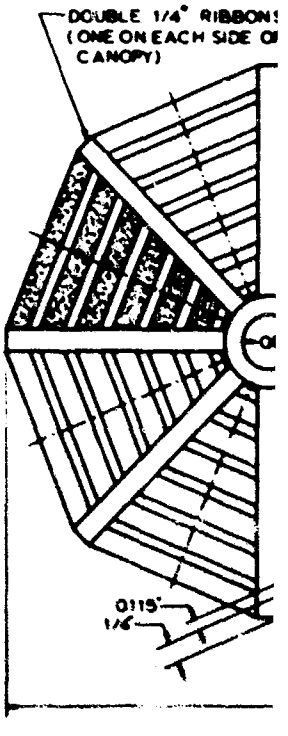


FIG 10-2 FLEXIBLE CANOPY
RIBBON PARACHU
(25% GEOME

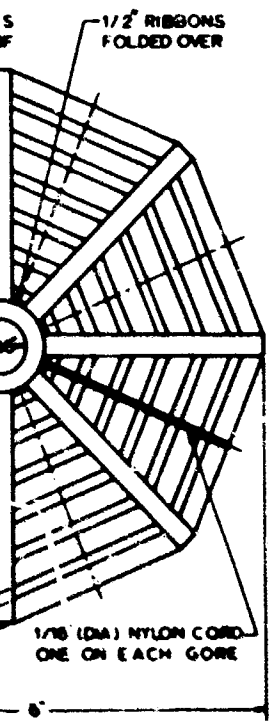


DESIGN FOR SPIKED
TE CONFIGURATION
TRIC POROSITY)

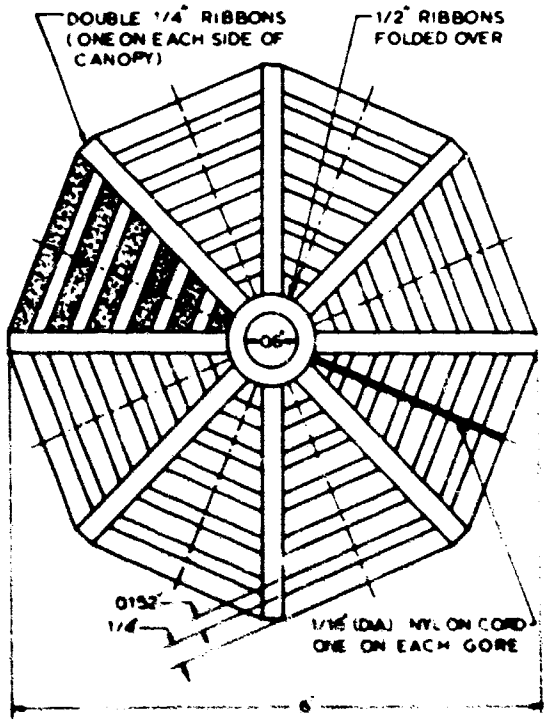


FIG 10-3 FLEXIBLE CANOPY DESIGN FOR SPIKED
RIBBON PARACHUTE CONFIGURATION
(30% GEOMETRIC POROSITY)

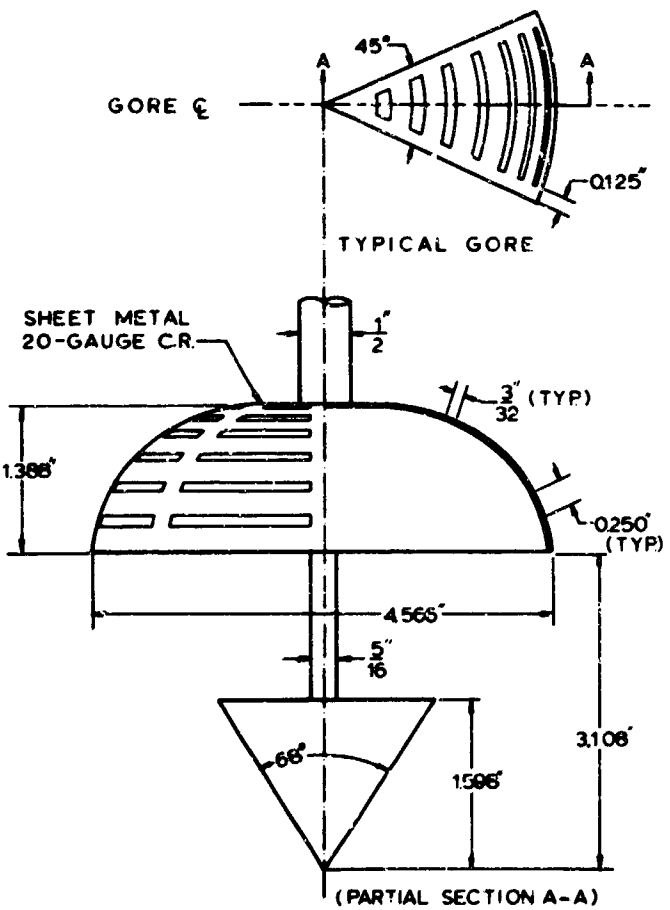


FIG 10-4. SPIKED RIBBON PARACHUTE CONFIGURATION (20% POROSITY)

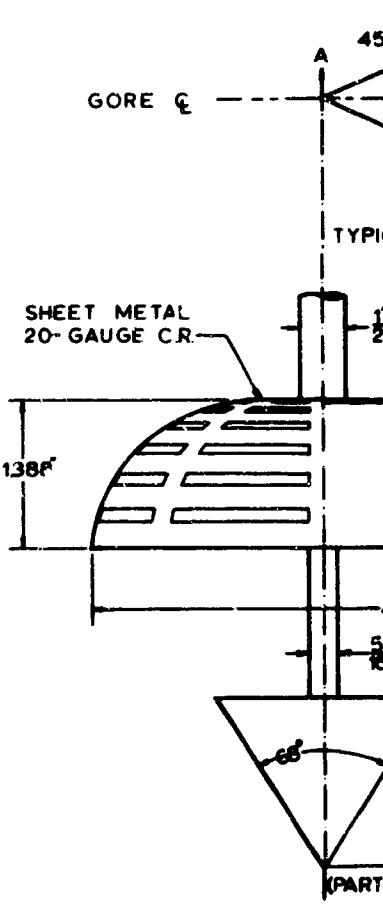


FIG 10-5. SPIKED RIBBO CONFIGURATION (2

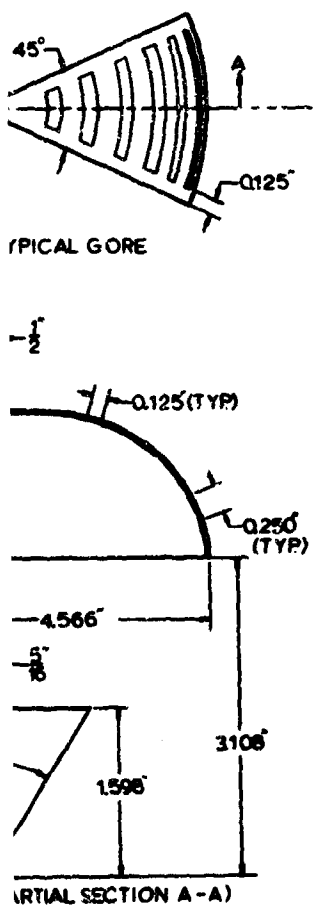


BON PARACHUTE
(25% POROSITY)

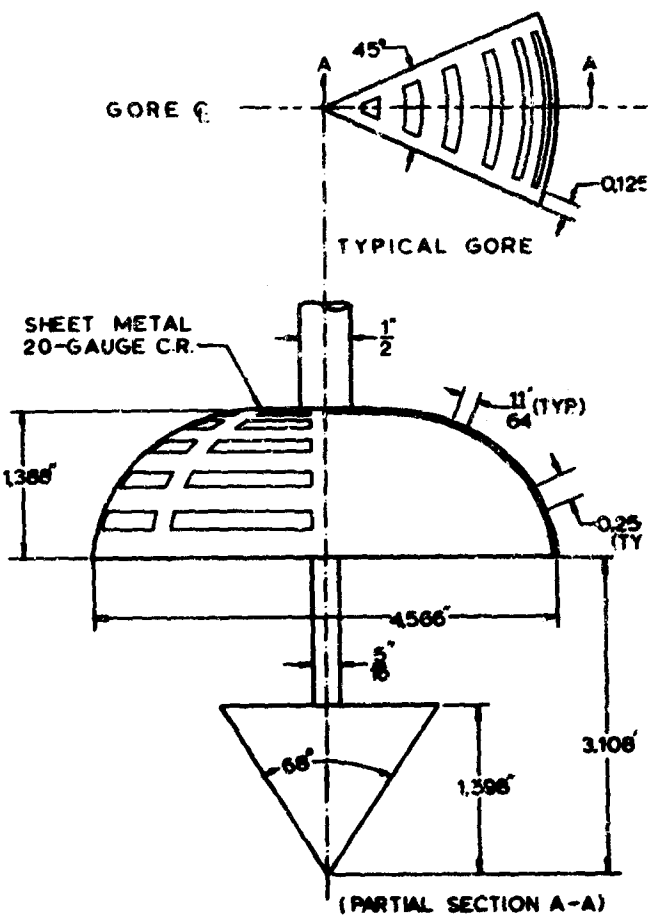


FIG 10-6 SPIKED RIBBON PARACHUTE
CONFIGURATION (30% POROSITY)

## 8.0 Gliding Aerodynamic Decelerator

The objective of this study is to develop a self-inflating aerodynamic decelerator which has a lift to drag ratio of 2. Such an L/D ratio gives an angle of attack of 63.5° between the longitudinal axis and the relative wind; thus, the parachute would glide at an angle of 26.5° to the horizon during descent.

As first step in the search for such a decelerator, the parachutes investigated in Ref 1 were reviewed and it was found none satisfied the L/D = 2 requirement. Therefore new shapes were studied which consisted essentially of rigid models made of balsa wood modified with modelling clay. With such models, configurations were found which met the requirement of L/D = 2, as reported in Progress Report No 18, Sec 9.3.3.

Work during the present reporting period has been devoted to the development of forms which can be built of textile segments.

Promising configurations have been found and it is expected that actual textile models will be built during the next reporting period.

### REFERENCES

1. Heinrich, H. G., and Haak, E. L.: Stability and Drag of Parachutes with Varying Effective Porosity (to be published as an ASD Technical Report).

## 9.0 Ribbon Grids for Supersonic Flow

### 9.1 Introduction

In earlier progress reports under Project No 4, studies were described which attempt to establish the relationship between air permeability and effective porosity of cloths and screens for various densities. These studies continue under that project.

The objective of this study is to investigate the behavior of ribbon and grid configurations tested at pressure differentials below and slightly above the critical pressure ratios which give sonic flow through the grids. Tests are also being made to determine the effects of design and structural deformation on effective porosity.

The test equipment has been described in detail in Progress Reports No 16, Sec 3.4.3, and No 17, Sec 10.2.2.

### 9.2 Experiments

During this reporting period, porosity tests and data reduction were completed on the set of ribbon configurations made from steel shim stock which were listed in Table 13-1, Progress Report No 18 with the exceptions of the 5 - 1/4 inch ribbon, the 3 - 5/8 inch ribbon and the 2 - 3/8 inch ribbon configurations. The flow rate of these three models was too high to measure with the available facility.

A series of tests was also made on a set of corresponding models made from MIL-R-5608B, Class A, nylon ribbon of 1/4 inch, 3/8 inch, and 5/8 inch widths. When these models were tested, it was observed that the ribbons deformed beyond the side walls of the test holder which had been used for the steel models (Fig 13-1), allowing air to escape and causing a change in the configuration of the model. To prevent this, side walls were added to the test holder (Fig 13-2). No data was obtained for

the 9- and 10- 1/4 inch ribbon configurations, because of instability of the ribbons during testing, together with failure of one or more ribbons in each configurations.

## 9.3 Results

Figures 13-3 through 13-5 present the effective porosity of the eleven steel ribbon configurations tested as a function of differential pressure at sea level density. These graphs include results presented in Figs 13-4 and 13-5 of Progress Report No 18. Figure 13-5 shows data from tests run at two different times. It is seen that repeatability is excellent.

The effective porosities of the nine nylon ribbon configurations tested as a function of pressure differential at sea level density are presented in Figs 13-6 through 13-8. Again, Fig 13-6 shows good repeatability of test results for these flexible models.

Figures 13-9 and 13-10 present comparisons of results of nylon and steel ribbon configurations. We see from these comparisons that for low pressure differentials ($\Delta p/\Delta p_{cr} \cong 0.025$) steel and nylon models with the same geometric porosity have approximately the same effective porosity. However, as the pressure differential increases, the effective porosity of the nylon models becomes greater than for the steel models, until at $\Delta p/\Delta p_{cr} \cong 1.0$ the nylon model has approximately the same effective porosity as a steel model with a geometric porosity twice that of the nylon model. From observation of the tests, this is attributed to two main factors. First, at high pressure ratios the nylon ribbons cup (Fig 13-11), causing a decrease in projected width of the ribbon to approximately one-half its unstressed width. Secondly, the nylon ribbons show a considerable increase in length at high pressure ratios. It appears that the cupping of the ribbons is the most significant factor in the increase of effective porosity with higher pressure ratios.

In view of the circumstances indicated above, the fact that the nylon ribbon grids show about twice as much effective porosity as the steel ribbons may be a consequence of the form and size of the model holder. This ratio of "2" would probably change with a change of model holder.

## 9.4 Proposed Work

Models of grid configurations with various shapes and opening sizes are being prepared from steel shim stock and will be tested during the next reporting period. Models of the same configurations will be made from nylon ribbons and tested to determine the effect of model deformation on effective porosity. These models all have a geometric porosity of 0.250, so it will be possible to simultaneously investigate the effects of grid design on effective porosity.

Tests will also be made on all nylon and steel ribbon and grid models at density ratios $\sigma < 1$ using the facility described in Sec 3.4.2 of Progress Report No 18.

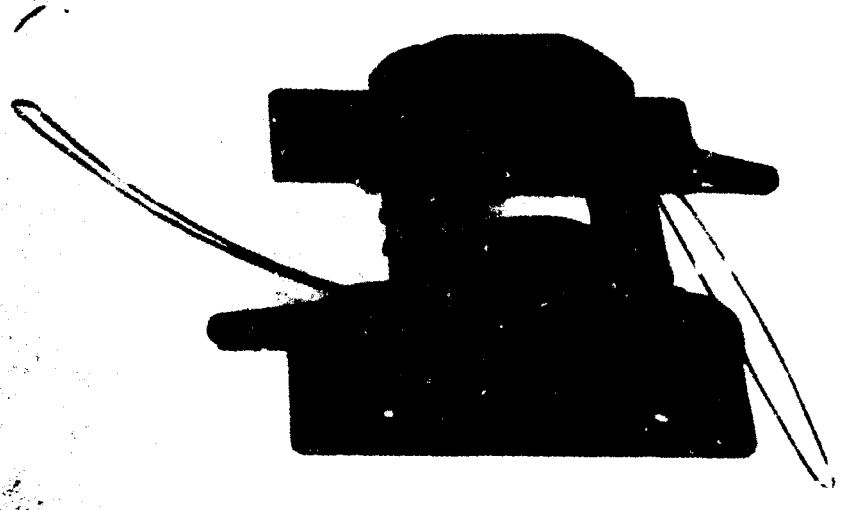

FIG 13-1. TEST HOLDER FOR STEEL RIBBON MODELS.

FIG 13-2. TEST HOLDER FOR NYLON RIBBON MODELS.

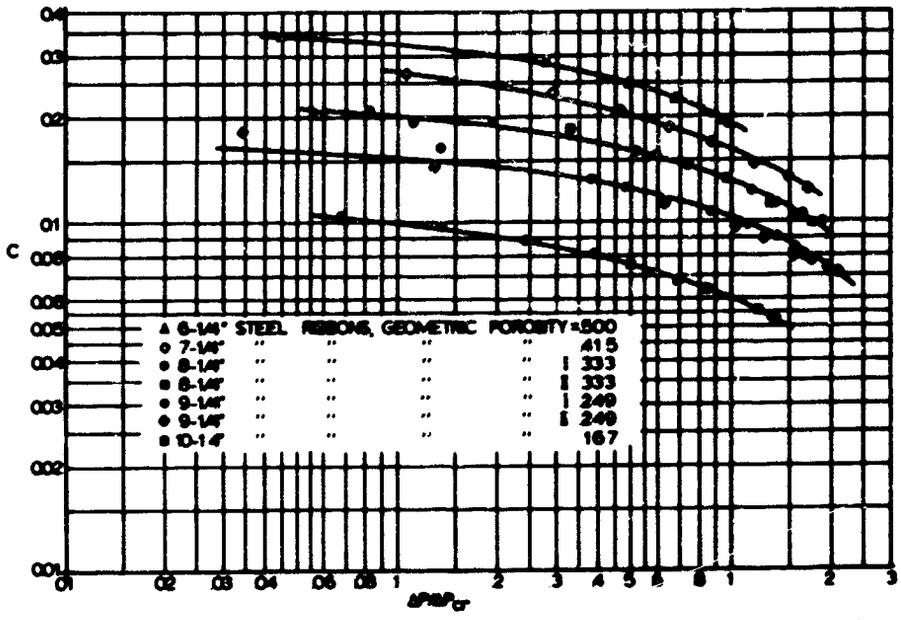


FIG 13-3 EFFECTIVE POROSITY OF FIVE STEEL RIBBON GRID CONFIGURATIONS AS A FUNCTION OF DIFFERENTIAL PRESSURE

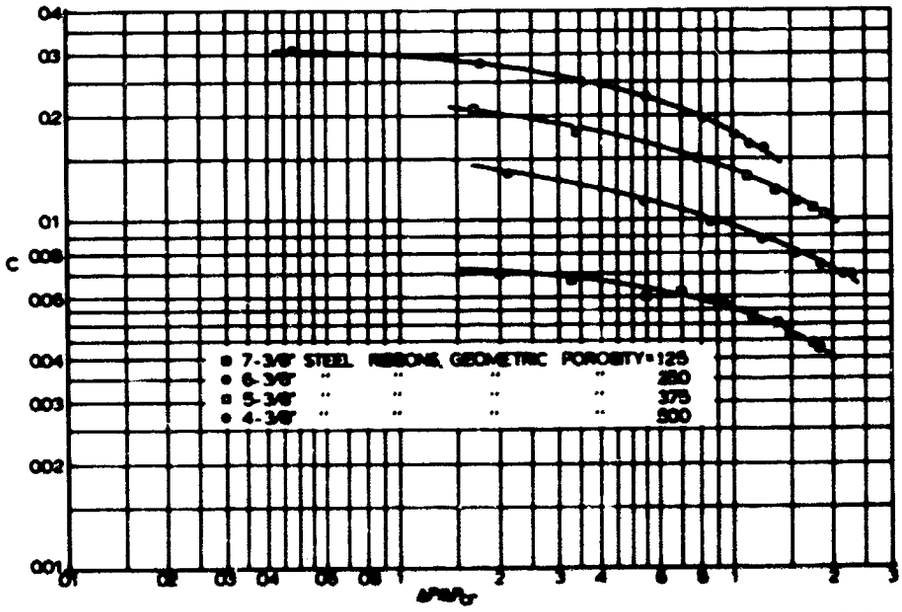


FIG 13-4 EFFECTIVE POROSITY OF FOUR STEEL RIBBON GRID CONFIGURATIONS AS A FUNCTION OF DIFFERENTIAL PRESSURE

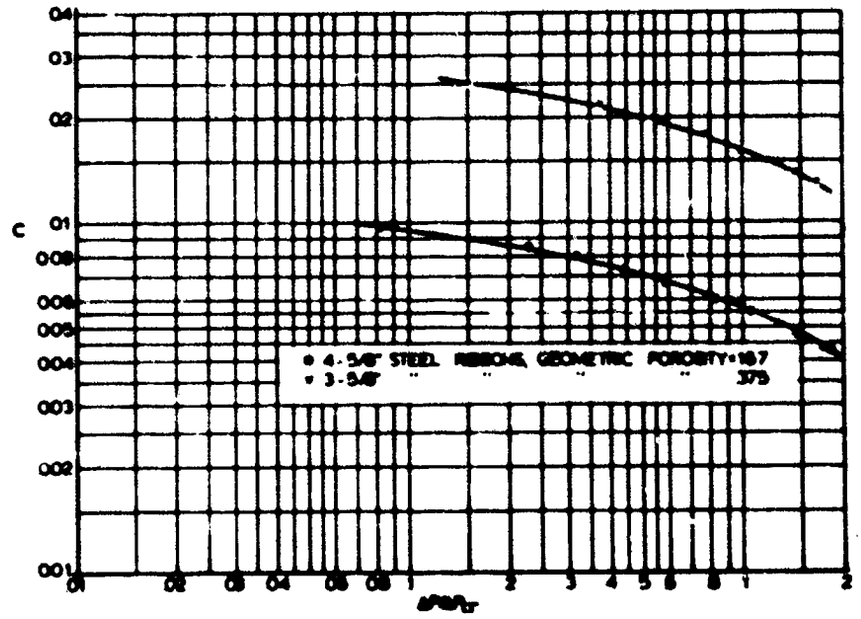


FIG 13-5 EFFECTIVE POROSITY OF TWO STEEL RIBBON GRID CONFIGURATIONS AS A FUNCTION OF DIFFERENTIAL PRESSURE

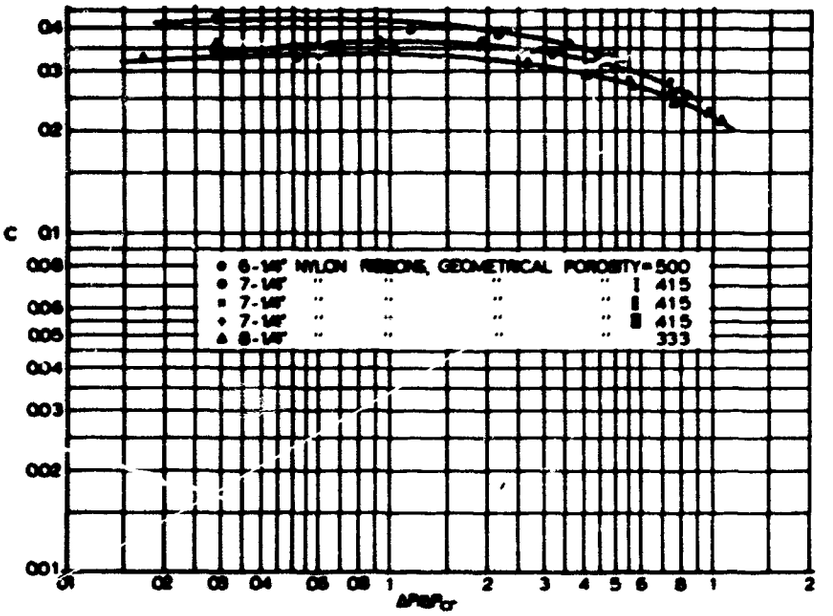


FIG 13-6 EFFECTIVE POROSITY OF THREE NYLON RIBBON GRID CONFIGURATIONS AS A FUNCTION OF DIFFERENTIAL PRESSURE

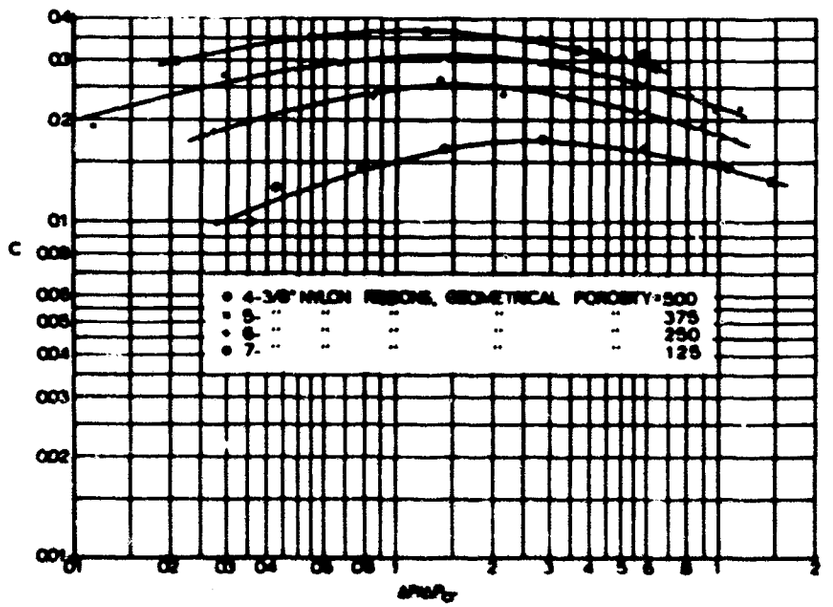


FIG 13-7 EFFECTIVE POROSITY OF FOUR NYLON RIBBON GRID CONFIGURATIONS AS A FUNCTION OF DIFFERENTIAL PRESSURE

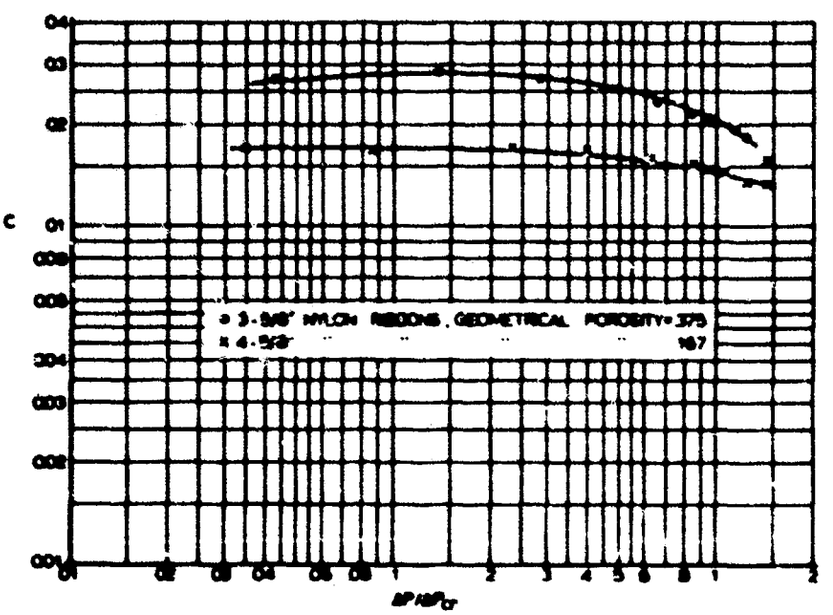


FIG 13-8 EFFECTIVE POROSITY OF TWO NYLON RIBBON GRID CONFIGURATIONS AS A FUNCTION OF DIFFERENTIAL PRESSURE

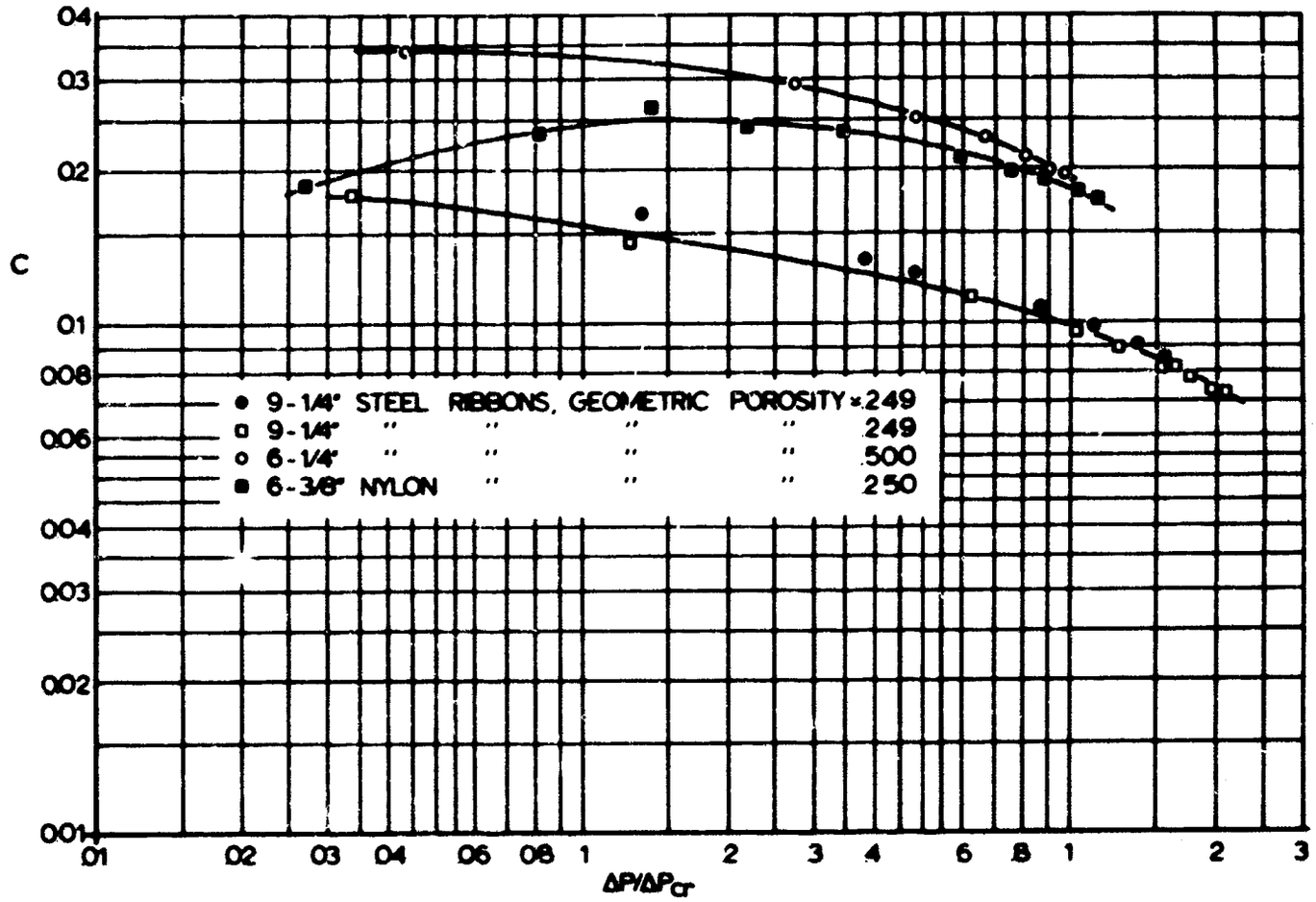


FIG 13-9. COMPARISON OF EFFECTIVE POROSITY OF NYLON AND STEEL RIBBON GRIDS

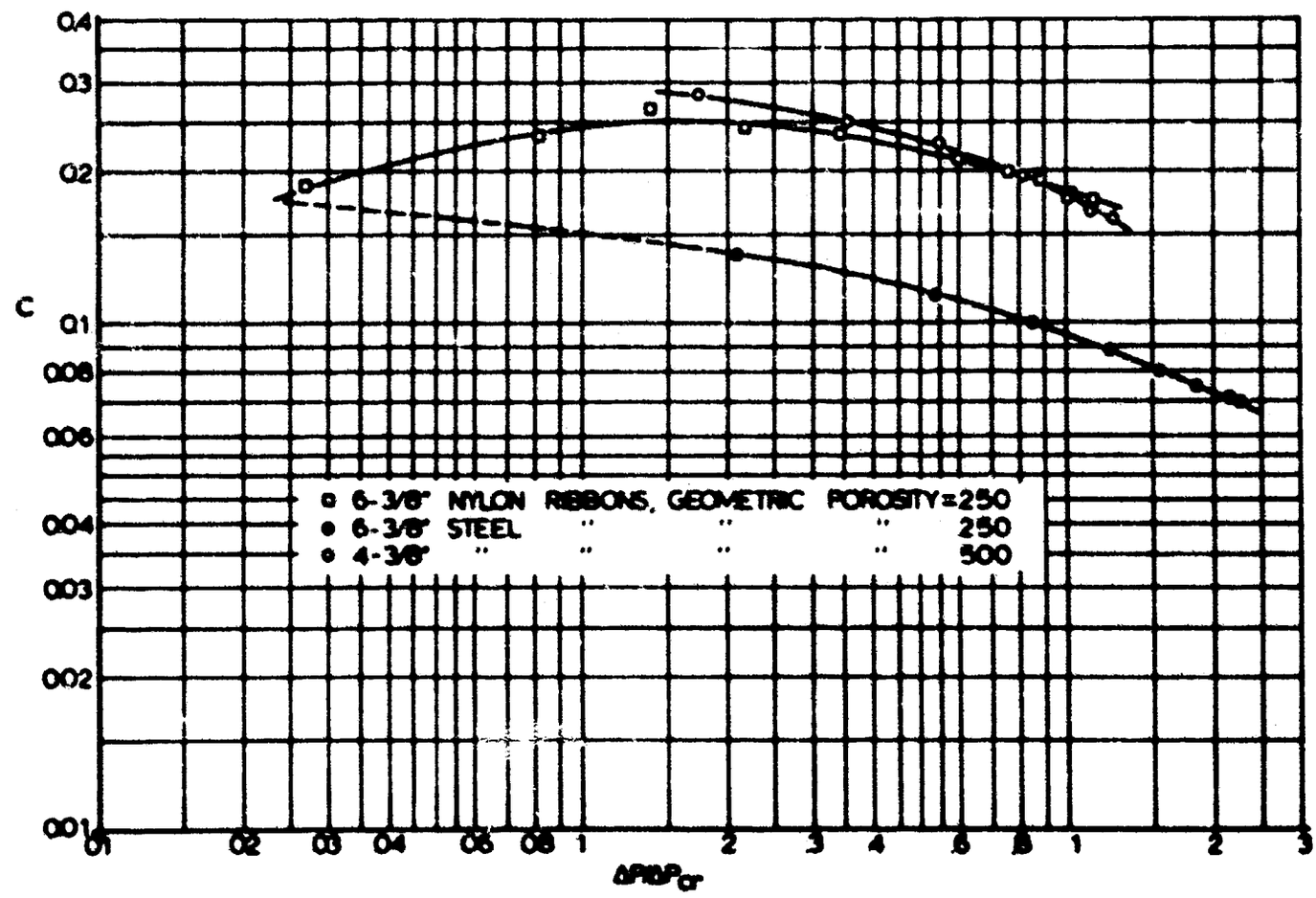


FIG 13-10. COMPARISON OF EFFECTIVE POROSITY OF NYLON AND STEEL RIBBON GRIDS

A. $\Delta p/\Delta p_{cr} \cong 0.6$

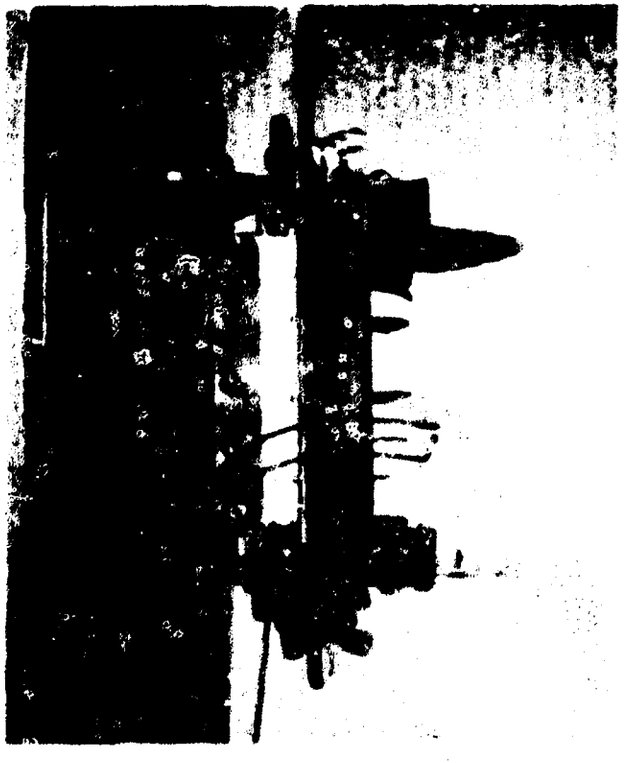

B. $\Delta p/\Delta p_{cr} \cong 1.0$

C. $\Delta p/\Delta p_{cr} \cong 1.5$

FIG 13-11. CUPPING OF RIBBONS AT HIGH PRESSURE RATIOS

## 10.0 Study of Flow Patterns of Aerodynamic Decelerators by Means of the Surface Wave Analogy

### 10.1 Introduction

Progress Report No 18 indicated the completion of the main components of the water channe. by the sub-contractor and reported that the detail design of some auxiliary components and items of instrumentation, including a multi-probe carriage with traversing mechanism and depth survey apparatus and shadowgraph and Schlieren systems, was in progress.

### 10.2 Final Assembly of Water Channel

In the early part of the present period, the final assembly of the water channel was completed. This involved mounting and anchoring in place the main structural framework of the water channel and connecting and sealing the various flanged sections which form part of the water circuit. The 15 ft long, 52½ in. wide and ½ inch thick high grade plate glass (with surfaces estimated accurate to ± 0.001 in.) forming the test section channel floor was mounted on 54 adjustable plexiglass jack pads suitably spaced in the longitudinal and lateral direction.

For levelling the glass surface, the supporting frame was initially levelled and the table was filled to about 1 inch of water. A depth micrometer was used to check the depth at various points and the jack pads were systematically adjusted until the glass surface was within ± 0.003 in.

The method of sealing the glass was somewhat similar to that used previously in the water tow test facility as described in Progress Report No 10, Sec 6.2.1 and Fig 7-4. However, when water circulation tests indicated a number of leaks around the glass edges, it was necessary to add flexible rubber tubing squeezed between the glass edges and the channel side walls and

running the full length of the glass plate on both sides. 3-M Super Weatherstrip adhesive was used for the rubber to glass seal and aquarium cement was used for filling the void spaces.

At the downstream end of the channel, a $\frac{1}{4}$ inch thick $52\frac{1}{8}$ inch wide and 36 inch long aluminum plate was added to form an extension of the flow channel beyond which the water sheet falls into the 500 gallon capacity reservoir.

At the upstream end of the channel a $\frac{1}{4}$ inch thick aluminum plate $52\frac{1}{8}$ inch wide and 18 3/4 inches long was hinged to the top plate of the nozzle approach section. By changing the height of the opening at the discharge end, it is possible to vary the water depth up to 2 inches. The water flow velocity and corresponding simulated Mach number is controlled by means of the 6 inch Walworth gate valve on the discharge side of the constant speed centrifugal pump.

Initial runs of the water channel were carried out at a water depth of 0.5 inches. It was noticed that the slight roughness of the steel angles forming the channel sides and the small irregularities at the corners created disturbances which appeared in the flow as weak oblique waves (simulated Mach waves). To reduce this effect and obtain sharply defined corners for the water flow section, plexiglass strips $\frac{1}{2}$ inch wide and $2\frac{1}{2}$ inches high were attached to the steel angles along the length of the channel to form the effective sides of the water flow section. This arrangement resulted on a noticeable improvement of the flow.

The initial runs indicated also that, despite the use of a flexible joint between the pump and the water ducting and massive rigid structure, a certain amount of vibration from the electric motor and pump is transmitted to the water ducting and nozzle plate producing random irregularities on the surface of the water. Efforts will be directed towards stiffening the nozzle plate to reduce the amplitude of the vibration and towards reducing as far as possible the vibration of the channel structure.

It is of interest to note that, for the shadowgraph and Schlieren photographic systems used, it is possible to minimize random changes in the flow images obtained by using relatively long exposures.

## 10.3 Instrumentation

### 10.3.1 Point by Point Depth Probe

In the later part of the reporting period, attention was directed to the instrumentation of the water channel. A standard micrometer caliper head with 0.001 inch graduations was fitted with a needle probe and mounted on the multi-probe carriage to form a point by point depth survey system. The same type of micrometer caliper head will be adapted to carry pressure probes to be used for water flow surveys.

### 10.3.2 Shadowgraph System

A simple shadowgraph system consisting of a light source, a 14 inch diameter plastic Fresnel lens of 14 inch focal length and a frosted glass screen was developed. Figure 14-1 presents some sample shadowgraphs obtained with this system. It is felt that the shadowgraph method, especially when complemented with other flow visualization techniques, will prove very valuable in the study and interpretation of flow patterns, particularly for the more complex configurations such as the supersonic parachute of Project No 7.

### 10.3.3 Schlieren Systems

The development of a Schlieren system for the water channel has been initiated and some progress has been made. The system uses the components of the shadowgraph system with the addition of another identical Fresnel lens, prism, and knife edges. Because a Schlieren system would be sensitive to gradual depth changes for which a shadowgraph system is not responsive,

it will be a valuable tool in the study of the water depth throughout the whole field of flow.

10.3.4 Water Depth Distribution Around Models

In order to be able to calculate, by analogy, the pressure distribution on the surface of a given body in air, it is necessary to determine, experimentally, the water depth distribution around the hydrodynamic model. Tests were conducted to develop a simple experimental technique which would give the water depth profile around the fixed model immersed in the running water. A technique using photographic paper wrapped around the model and exposed, for a brief period, to external lighting had been tried with an earlier water channel. This technique necessitates conducting the tests in a dark room, which is not convenient in the present laboratory.

Many tests were conducted using commercial water colors and various water soluble dyes such as Methylene Blue, Saffranine, Aniline Blue, and Eosin applied to the model surface. These tests were to determine certain desirable characteristics, such as the time required for the dye to wash away from the immersed region and the sharpness of definition of the water mark. As a result of these tests, it was found that aqueous and alcoholic solutions of Eosin were very satisfactory for the proposed application, giving a sharply defined outline within a few seconds depending on the concentration of the dye and surface preparation of the model.

It must be noted, of course, that the capillary attraction of the model wall for the water surface will raise the local height of the water level but it is hoped that satisfactory corrections for these effects may be applied.

It is planned to conduct tests on some reference models using the Eosin dye method developed and compare its results with direct measurements by means of the micrometric depth probe and-or pressure orifices connected to tubes in a manometer where capillary effects can be minimized.

10.4 Proposed Work

In the next reporting period, it is proposed to make a final realignment of the channel and quide rails with a final check and readjustment of the glass surface if necessary.

As mentioned in Sec 10.2 above, attempts will be made to reduce as far as possible the transmission of vibration to the water surface y stiffening the nozzle top plate and improving anti-vibration measures.

The development of the Schlieren system will be carried out as far as practicable.

After the final realignment of the channel and checks on the glass surface, calibration tests will be conducted and the necessary longitudinal and lateral velocity traverses will be taken. Special charts will be prepared showing the necessary channel settings such as valve opening and channel slope required to simulate a given Mach number for a given initial water depth.

Simultaneously, tests to determine the water depth distribution and simulated pressure distribution for some specific configurations of stable spiked supersonic parachutes at M = 2.0 as given in the supplement to Progress Report No 13 will be conducted and the method evaluated. These tests will be supplemented by shadowgraph and Schlieren visualizations when desirable.

A. CIRCULAR CYLINDER

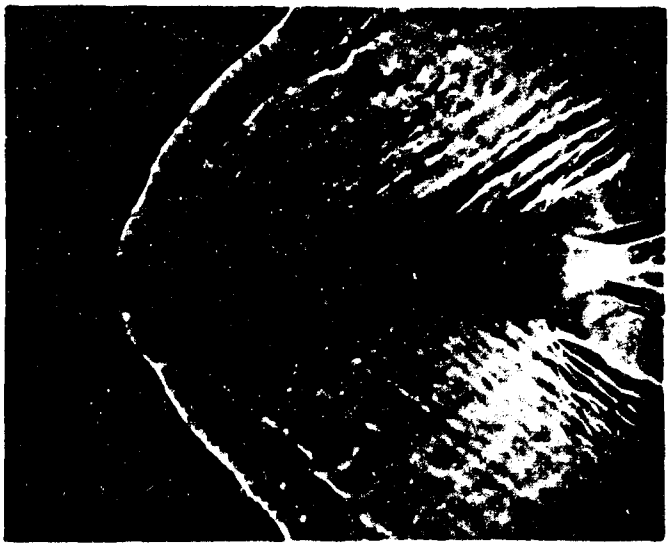

C. OGIVE CYLINDER

FIG 14-1. SAMPLE SHADOW
MACH NUMBER N

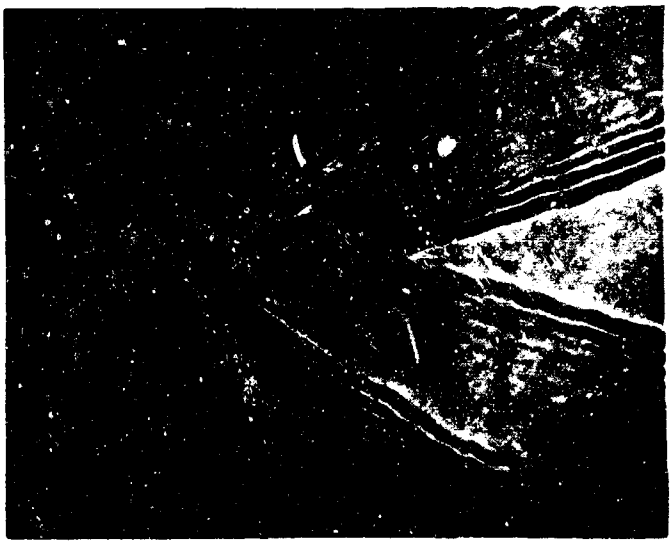

B. DIAMOND AIRFOIL

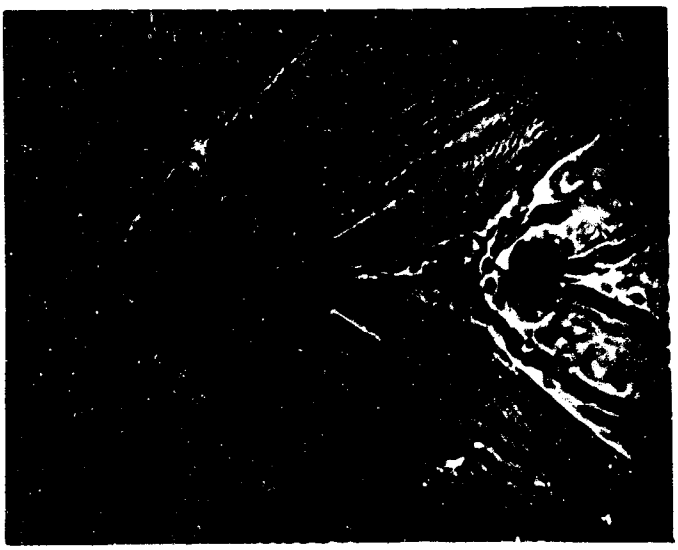

D. OGIVE CYLINDER AND CIRCULAR CYLINDER COMBINATIONS.

WGRAPHS IN WATER CHANNEL.
NOT DETERMINED.

Project No 16

## 11.0 Stress Analysis of the T-10 Troop Parachute

Progress Report No 18 presented an analytical method for obtaining the stress distribution over a T-10 extended skirt troop parachute in steady descent based on a known pressure distribution over the canopy. This completed the first objective of this study.

The method presented was general enough so that it can be applied to any other type of canopy with only minor modifications. The method also appears to be applicable to finding the stress distribution in a canopy during the opening process. These additional efforts will be pursued upon authorization of the Procuring Agency.

## APPENDIX

The authors of this report who are listed on the front page wish to acknowledge the accomplishments and assistance of the following personnel:

Clerical Staff:

E. Zembergs, Sr. Engineering Assistant
Beverly M. Broers, Secretary

Graduate Students:

R. O. Bailey, Research Assistant
D. J. Eckstrom, Research Assistant
S. R. Hess, Research Assistant
E. M. Linhart, Research Assistant
W. K. Lockman, Research Assistant
D. J. Monson, Research Assistant
J. J. Paulson, Research Assistant
A. Perlbachs, Research Assistant
L. W. Rust, Research Fellow
R. E. Schaller, Research Assistant

Undergraduate Students:

J. Baker, Engineering Assistant
J. S. Bratly, Engineering Assistant
J. W. Bushard, Engineering Assistant
J. M. Carlson, Engineering Assistant
D. D. Evenson, Engineering Assistant
R. W. Friestad, Engineering Assistant
L. R. Jamison, Engineering Assistant
H. R. Kokal, Engineering Assistant
D. A. MacLean, Engineering Assistant
D. E. McGee, Engineering Assistant
W. R. Mueller, Engineering Assistant
T. C. Nietz, Engineering Assistant
E. H. Nierengarten, Engineering Assistant
D. R. Nordwall, Engineering Assistant
D. Pekarek, Engineering Assistant
R. O. Strom, Engineering Assistant
L. M. Timmons, Engineering Assistant

Machine Shop Personnel:

J. Taube, Laboratory Machinist
P. A. Huehnert, Wind Tunnel Mechanic